Exciton-phonon coupling in molecular crystals: Synergy between two intramolecular vibrational modes in quaterthiophene single crystals

Leonardo Silvestri,[1,a)] Silvia Tavazzi,[1] Peter Spearman,[1] Luisa Raimondo,[1] and Frank C. Spano[2]
[1]*Dipartimento di Scienza dei Materiali, Università degli Studi di Milano Bicocca, via Cozzi 53, I-20125 Milano, Italy*
[2]*Department of Chemistry, Temple University, Philadelphia, Pennsylvania 19122, USA*

(Received 29 January 2009; accepted 16 May 2009; published online 16 June 2009)

Exciton-phonon (EP) coupling in molecular crystals is investigated in the case where two intramolecular vibrational modes are involved and a theoretical model is presented which applies when one of the modes is strongly coupled to crystal excitons. The model is used to simulate the low energy portion of the absorption spectra of quaterthiophene (4T) single crystals, for which we find it appropriate to consider a low energy vibrational mode at 161 cm^{-1} and an effective strongly coupled high energy mode at 1470 cm^{-1}. Our numerical results demonstrate that the high energy mode renormalizes the excitonic band, thereby strongly affecting the environment seen by the low energy mode and the overall EP coupling regime. Numerical simulations also confirm the existence of the new coupling regimes "intermediate-I" and "strong-I" already introduced for oligothiophene aggregates [Spano *et al.*, J. Chem. Phys. **127**, 184703 (2007)], which arise as a consequence of the large effective mass of low energy excitons in 4T crystals. Comparison with experimental high resolution absorption spectra is also reported and shown to support the model predictions.
 [DOI: 10.1063/1.3151675]

I. INTRODUCTION

Optical properties of molecular aggregates and crystals have been widely studied in recent years mainly because such systems have large oscillator strengths and, by chemical substitutions, it is possible to tune their transition energies to cover the whole visible spectrum. These features are very interesting and are currently exploited in many organic-based devices such as solar cells and light emitting devices.[1–5]

Absorption and emission spectra of molecular crystals are dominated by excitons consisting of delocalized single molecule electronic excitations. The properties of excitons in such systems are strongly influenced by their coupling to intramolecular phonons, which give rise to the vibronic progressions typically observed in optical spectra. The conventional treatment of exciton-phonon (EP) coupling identifies different regimes by comparing the nuclear relaxation energy to a measure of the electronic interaction between molecules, usually taken to be the free-exciton bandwidth or, in the case of more than one molecule per unit cell, the free-exciton Davydov splitting (DS) W. For a single harmonic intramolecular vibrational mode of energy $\hbar\omega$, the nuclear relaxation energy is given by $\lambda^2\hbar\omega$, where λ^2 is the Huang–Rhys (HR) factor. In this case weak, intermediate and strong EP coupling corresponds to the three situations $\lambda^2\hbar\omega \ll W$, $\lambda^2\hbar\omega \sim W$, and $\lambda^2\hbar\omega \gg W$, respectively.[6,7] However, when describing emission or the low energy portion of the absorption spectra, such a classification is not accurate if, for the case $W \gg \lambda^2\hbar\omega$, the lowest energy exciton has a very high effective mass. In fact, the interactions between these low energy excitons are better described by the local band curvature than by the total bandwidth W. Focusing for simplicity our attention on crystals with two molecules per unit cell and two allowed excitonic bands, we can say that the conventional classification fails when $W \gg \lambda^2\hbar\omega$ and the lower band has a bandwidth Δ of the same order of magnitude as or less than the nuclear relaxation energy. For such a regime, which is not contemplated even in the more refined scheme introduced by McRae and Siebrand,[8] we showed that it is convenient to introduce two new EP regimes we called "intermediate-I" and "strong-I," appropriate when $(4/\pi)\Delta \approx \lambda^2\hbar\omega \ll W$ and $(4/\pi)\Delta \ll \lambda^2\hbar\omega \ll W$, respectively, while the conventional weak coupling results when $\lambda^2\hbar\omega \ll (4/\pi)\Delta$.[9] For the sake of clarity, we point out that the model aggregate we used in Ref. 9 had a single excitonic band, so that the quantity $J_c\pi^2$, J_c being the excitonic band bottom curvature in units of energy, played the same role as Δ here.[10] We can describe the intermediate-I (strong-I) regime as a situation in which, according to the conventional classification, lower band excitons would be in an intermediate (strong) EP coupling regime, while upper band excitons would be in a weak coupling regime. In our previous paper[9] we developed a model herringbone aggregate with a single coupled intramolecular mode and applied it to quaterthiophene (4T) considering the lowest energy intramolecular vibrational mode at 161 cm^{-1}. In that way we could identify clear signatures of the new regimes in the low energy portion of high resolution experimental absorption spectra of 4T single crystals.[11] In the same paper we pointed out that the

a)Electronic mail: leonardo.silvestri@mater.unimib.it.

flattening of the excitonic band dispersion could be enhanced by other vibrational modes, pushing the system toward the new regimes.

In this work we present a theoretical model to describe EP coupling in a crystal with long-range interactions and two strongly coupled intramolecular vibrational modes. The model is applied to 4T crystals of the low-temperature polymorph, considering the low energy mode at 161 cm^{-1} and a high energy effective mode at 1470 cm^{-1}. By numerical simulation of the low energy portion of the 4T absorption spectrum, we demonstrate first that the new strong-I and intermediate-I regimes apply to crystals, and in particular to 4T, as well as to aggregates. Second, and even more importantly, we demonstrate that if more than one vibrational mode is present, they influence each other and synergistic effects cannot be neglected when identifying the EP coupling regime of the system. In particular the 1470 cm^{-1} mode of 4T is found to renormalize the free-exciton bands, pushing the crystal from the weak EP coupling regime into the intermediate-I to strong-I regime.

The paper is organized as follows. In Sec. II we present the 4T crystal, the theoretical model to describe it, and the excitonic band calculations. In Sec. III we present the numerical results showing the dramatic effect of adding the high energy mode and compare them to experimental results. In Sec. IV we analyze the calculated two-mode absorption spectra in terms of the vibronic basis set presented in Sec. II. Section V is devoted to the conclusions.

II. CRYSTAL MODEL

In this section we present a model which describes the optical properties of the low-temperature polymorph of 4T.[12] Quaterthiophene is a widely studied molecular material[11–21] which possesses interesting properties for both applications and fundamental research,[22] since it can be regarded as a model system for many molecular materials crystallizing in a herringbone packing arrangement such as oligothiophenes[15,23] and *p*-oligophenylene vinylenes.[24,25] The crystallographic structure of the low-temperature 4T polymorph is monoclinic with four molecules per unit cell, whose axes are $a=6.09$ Å, $b=7.86$ Å, and $c=30.48$ Å, the angle β between a and c being 91.8°.[12] Since different names can be found in the literature for the axes of the monoclinic unit cell, for the sake of clarity we denote the monoclinic axis as the b axis and the longest axis as the c axis. The accessible face for optical measurements is the ab plane. In the following we will make use of the orthogonal coordinate system defined by a, b and the reciprocal cell axis c^* oriented along $\mathbf{a}\times\mathbf{b}$.

Quaterthiophene molecules in the crystal are planar and present C_{2h} symmetry with the twofold axis of rotation perpendicular to the molecule plane, defined as the N axis in the molecular frame. All of the four inequivalent molecules in the unit cell belong to the same crystallographic species and can be obtained one from another by applying one of the symmetry operations of the crystal space group $P2_1/c$. The first allowed molecular transition has B_u symmetry and its transition dipole moment lies in the molecular plane LM, mostly along the long molecular axis L. Due to the arrangement of the molecules, in the crystal the transition dipole moment is directed mainly along c^* but also has components along a and along the monoclinic axis b. It follows that in the accessible ab plane molecular dipole moment projections are arranged in a herringbone fashion. Interaction between molecules in the crystal gives rise to Frenkel excitons which can be described by the Davydov theory of molecular excitons.[26] In 4T crystals we find four excitonic bands, only two of them being optically allowed, and the free exciton DS between the two allowed bands is, as we will see, about 0.9 eV or 7200 cm^{-1}. This is quite a large value, but it should not be surprising, as first pointed out by Petelenz and Andrzejak[27] in the case of sexithiophene crystals. We further notice that the interaction between adjacent ab planes in the crystal is weak, compared to the interactions between molecules in the ab plane, so that in the following we will consider a single ab plane as a model for the full three dimensional (3D) crystal.[22] In this case we have that any two dimensional (2D) cell contains two translationally inequivalent molecules connected by a screw symmetry. The 2D factor group is therefore C_2 and it gives rise to two optically allowed Davydov bands at $\mathbf{k}=0$: The lower band with A symmetry and transition dipole moment along b, the upper band with B symmetry and transition dipole moment in the ac plane. We will further discuss the 2D approximation in Secs. II A and II B, but we anticipate that it is correct as long as one considers normal incidence absorption spectra. For this reason in the present paper we will only consider normal incidence spectra and we will always refer to their a- and b-polarized components; it is however understood that at oblique incidence the absorption spectrum decomposes into uncoupled ac- and b-polarized components.

Excitons in 4T are coupled with at least five intramolecular vibrational modes of energies 161, 333, 688, 1235, and 1551 cm^{-1}, respectively.[16] Since $W \gg \Sigma_{i=1}^{5} \lambda_i^2 \hbar\omega_i$, i labeling the vibrational modes, according to the conventional classification the crystal should be described by the weak EP coupling approximation. In that regime crystal eigenstates can be approximated by Born–Oppenheimer (BO) products of a free exciton and a phonon wave function. We therefore expect the low energy part of the normal incidence absorption spectrum to consist of a b-polarized (0-0) origin followed by two weak degenerate (0-1) absorption bands, having b- and a-polarizations, respectively, with a low energy edge lying exactly 161 cm^{-1} above the origin and a shape determined by the free exciton band structure. This is because such (0-1) bands originate from crystal states obtained by adding to the free excitons with wave vector $\mathbf{k}$ a single delocalized low energy intramolecular phonon with wave vector $\mathbf{q}=-\mathbf{k}$. In the weak EP coupling approximation, (0-1) bands are optically allowed through a very weak Herzberg–Teller (HT) coupling[28] to the allowed zero phonon states at $\mathbf{k}=0$, which explains why b-polarized and a-polarized replicas are expected to be nearly degenerate. In fact, experimental spectra show that the two (0-1) replicas are well defined peaks, separated in energy by 25–30 cm^{-1} depending on the measured sample.[11] We interpret such behavior as a clear signature of a new regime in which, as already mentioned,

lower Davydov excitons are nearly degenerate and, as a consequence, the coupling between the (0-0) origin and *b*-polarized (0-1) states cannot be treated as a weak perturbation.[9,29] In the following we will present a model to describe the low energy absorption of molecular crystals in the strong-I and intermediate-I regimes, including two intramolecular vibrational modes. In particular we will include the low energy mode at 161 cm^{-1} and an effective mode at 1470 cm^{-1} which mimics the effect of all the other vibrational modes.[14,18]

A. Hamiltonian and absorption

We consider a 2D crystal composed of N unit cells, each containing a pair of two-level molecules. Each molecule has a ground (A_g) and a singly excited electronic state (B_u) with transition frequency $\omega_{0\text{-}0}$. Crystal cells are labeled by the integer vector $\mathbf{n}=(n_a,n_b)$ with $n_a=0,\ldots,N_a-1$, $n_b=0,\ldots,N_b-1$, and $N=N_aN_b$. Inequivalent molecules inside each cell are labeled by the index $\alpha=1,2$; we also denote by $\mathbf{r_n}=n_a\mathbf{a}+n_b\mathbf{b}$ the position of crystal unit cell $\mathbf{n}$ and by $\boldsymbol{\rho}_\alpha$ the position of the αth molecule inside the cell. The electronic transition is linearly coupled to two totally symmetric intramolecular vibrations: A low energy mode of frequency ω_0 and a high energy mode of frequency ω_1. The ground and excited nuclear potentials for a given molecule are taken to be shifted harmonic potentials with identical curvature and HR factors λ_0^2 and λ_1^2 for the two modes, respectively. Moreover, the high energy vibration is assumed to always reside on the electronically excited molecule, i.e., we are treating mode 1 in the vibronic or single particle approximation. The limits of validity of the above approximation will be discussed in Sec. IV. van der Waals interactions within a crystal induce the usual gas-to-crystal shift D, which is taken to be independent of the molecular site. Moreover, an excited molecule α inside cell $\mathbf{n}$ can resonantly transfer its energy to a β molecule at $\mathbf{m}$ via the excitonic coupling $J_{\alpha\beta}(\mathbf{n}-\mathbf{m})$. We will now consider the vibronic subspace spanned by states $|\mathbf{n},\alpha,\tilde{\mu}\rangle$, in which the αth molecule in cell $\mathbf{n}$ is electronically excited and $\tilde{\mu}$ quanta of the high energy vibration reside on it, while all other molecules remain unexcited and with no vibrations. Making use of Bloch combinations with wave vector $\mathbf{k}$ and imposing periodic boundary conditions, we finally write the dressed exciton states as

$$|\mathbf{k},\alpha,\tilde{\mu}\rangle \equiv \frac{e^{i\mathbf{k}\boldsymbol{\rho}_\alpha}}{\sqrt{N}}\sum_{\mathbf{n}} e^{i\mathbf{kn}}|\mathbf{n},\alpha,\tilde{\mu}\rangle, \tag{1}$$

with

$$\mathbf{k} \equiv \left(\frac{k_a}{N_a}\frac{2\pi}{a},\frac{k_b}{N_b}\frac{2\pi}{b}\right)$$

and

$$\begin{cases} k_j=-N_j/2+1,\ldots,0,\ldots,N_j/2, & \text{if } N_j \text{ is even} \\ k_j=-(N_j-1)/2,\ldots,0,\ldots,(N_j-1)/2, & \text{if } N_j \text{ is odd} \\ j=a,b \end{cases}. \tag{2}$$

The crystal Hamiltonian then reads[9,30]

$$H = H_{\text{vib}} + \hbar\omega_0\sum_{\mathbf{q},\alpha} b^\dagger_{\mathbf{q},\alpha}b_{\mathbf{q},\alpha} + \lambda_0^2\hbar\omega_0 + H_{\text{na}}, \tag{3}$$

where

$$H_{\text{vib}} = \hbar\omega_{0-0} + D + \sum_{\mathbf{k},\alpha,\tilde{\mu}} \tilde{\mu}\hbar\omega_1|\mathbf{k},\alpha,\tilde{\mu}\rangle\langle\mathbf{k},\alpha,\tilde{\mu}| + \sum_{\mathbf{k},\alpha,\beta,\tilde{\mu},\tilde{\nu}} S_{\tilde{\mu}0}S_{\tilde{\nu}0}\tilde{J}_{\alpha\beta}(\mathbf{k})|\mathbf{k},\alpha,\tilde{\mu}\rangle\langle\mathbf{k},\beta,\tilde{\nu}| \tag{4}$$

is the vibronic part of the Hamiltonian, which includes the coupling between free excitons and the high energy vibrational mode in a single particle approximation, and

$$H_{\text{na}} = \frac{\lambda_0\hbar\omega_0}{\sqrt{N}}\sum_{\mathbf{k},\mathbf{q},\alpha,\tilde{\mu}} [b^\dagger_{\mathbf{q},\alpha}|\mathbf{k},\alpha,\tilde{\mu}\rangle\langle\mathbf{k}+\mathbf{q},\alpha,\tilde{\mu}| + b_{\mathbf{q},\alpha}|\mathbf{k},\alpha,\tilde{\mu}\rangle\langle\mathbf{k}-\mathbf{q},\alpha,\tilde{\mu}|] \tag{5}$$

is the nonadiabatic part of the Hamiltonian which accounts for EP coupling involving the low-frequency intramolecular mode. In the above equations,

$$S^2_{\tilde{\mu}0} = \exp(-\lambda_1^2)\frac{\lambda_1^{2\tilde{\mu}}}{\tilde{\mu}!} \tag{6}$$

are the Franck–Condon overlap factors and

$$b_{\mathbf{q},\alpha} \equiv \frac{1}{\sqrt{N}}\sum_{\mathbf{n}} e^{-i\mathbf{qn}}b_{\mathbf{n},\alpha}, \quad b^\dagger_{\mathbf{q},\alpha} \equiv \frac{1}{\sqrt{N}}\sum_{\mathbf{n}} e^{i\mathbf{qn}}b^\dagger_{\mathbf{n},\alpha} \tag{7}$$

are operators creating and annihilating a delocalized low energy phonon, respectively, $b^\dagger_{\mathbf{n},\alpha}$ ($b_{\mathbf{n},\alpha}$) being creation (annihilation) operators corresponding to the low energy intramolecular vibrational mode on molecule α in cell $\mathbf{n}$. Low energy phonons have no dispersion and their wave vectors $\mathbf{q}$ are restricted by boundary conditions to the N nonequivalent values

$$\mathbf{q} \equiv \left(\frac{q_a}{N_a}\frac{2\pi}{a},\frac{q_b}{N_b}\frac{2\pi}{b}\right),$$

where q_j assumes the same set of values as k_j in Eq. (2). We have also defined

$$\tilde{J}_{\alpha\beta}(\mathbf{k}) = {\sum_{\mathbf{n}}}' e^{i\mathbf{k}(\mathbf{r_n}+\boldsymbol{\rho}_\alpha-\boldsymbol{\rho}_\beta)}J_{\alpha\beta}(\mathbf{n}), \tag{8}$$

where the primed summation (Σ') in Eq. (8) indicates that self-interaction must be excluded, i.e., if $\alpha=\beta$ then $\mathbf{n}\neq(0,0)$. Diagonalization of $\tilde{J}_{\alpha\beta}(\mathbf{k})$ at each $\mathbf{k}$ gives the purely excitonic bands. The phase factor $e^{i\mathbf{k}\boldsymbol{\rho}_\alpha}$ in Eq. (1) has been chosen so that for crystals with center of symmetry, such as 4T, $\tilde{J}_{\alpha\beta}(\mathbf{k})$ is real and symmetric about indices $\alpha\beta$.

It is convenient for future discussions to replace the dressed exciton basis set $|\mathbf{k},\alpha,\tilde{\mu}\rangle$ with the eigenfunctions $|\mathbf{k},dc,n\rangle$ of H_{vib} with eigenvalues $E^{\text{vib}}_{dc,n}(\mathbf{k})$. The new basis states, which diagonalize the vibronic term (4) of the Hamiltonian, have been labeled by their wave vector $\mathbf{k}$, the Davydov band dc they belong to, and by an index n numbering states in order of increasing energy. They are related to the dressed exciton states by

$$|\mathbf{k},\alpha,\tilde{\mu}\rangle = \sum_{dc,n} c_{\alpha,\tilde{\mu};dc,n}(\mathbf{k})|\mathbf{k},dc,n\rangle, \tag{9}$$

with coefficients satisfying the orthonormality conditions

$$\sum_{dc,n} c^{*}_{\alpha',\tilde{\mu}';dc,n}(\mathbf{k})c_{\alpha,\tilde{\mu};dc,n}(\mathbf{k}) = \delta_{\alpha\alpha'}\delta_{\tilde{\mu}\tilde{\mu}'}. \tag{10}$$

After substitution of expression (9) into Eq. (3), the crystal Hamiltonian takes the form

$$H = \sum_{\mathbf{k},dc,n} E^{\mathrm{vib}}_{dc,n}(\mathbf{k})|\mathbf{k},dc,n\rangle\langle\mathbf{k},dc,n| + \hbar\omega_0 \sum_{\mathbf{q},\alpha} b^{\dagger}_{\mathbf{q},\alpha}b_{\mathbf{q},\alpha} + \lambda_0^2\hbar\omega_0 + \frac{\lambda_0\hbar\omega_0}{\sqrt{N}} \sum_{\mathbf{k},\mathbf{q}} \sum_{dc,n} \sum_{dc',n'} [B^{\dagger}_{\mathbf{k},dc,n;\mathbf{k}+\mathbf{q},dc',n'}|\mathbf{k},dc,n\rangle\langle\mathbf{k} + \mathbf{q},dc',n'| + B_{\mathbf{k}+\mathbf{q},dc,n;\mathbf{k},dc',n'}|\mathbf{k}+\mathbf{q},dc,n\rangle\langle\mathbf{k},dc',n'|], \tag{11}$$

where the two operators

$$B^{\dagger}_{\mathbf{k},dc,n;\mathbf{k}+\mathbf{q},dc',n'} = \sum_{\alpha,\tilde{\mu}} c_{\alpha,\tilde{\mu};dc,n}(\mathbf{k})c^{*}_{\alpha,\tilde{\mu};dc',n'}(\mathbf{k}+\mathbf{q})b^{\dagger}_{\mathbf{q},\alpha} \tag{12}$$

$$B_{\mathbf{k}+\mathbf{q},dc,n;\mathbf{k},dc',n'} = \sum_{\alpha,\tilde{\mu}} c_{\alpha,\tilde{\mu};dc,n}(\mathbf{k}+\mathbf{q})c^{*}_{\alpha,\tilde{\mu};dc',n'}(\mathbf{k})b_{\mathbf{q},\alpha} \tag{13}$$

create and annihilate, respectively, an appropriate combination of delocalized low energy phonons coupling vibronic states with different wave vectors.

The above Hamiltonian can be represented in a BO basis set

$$|\mathbf{k},dc,n;n_{\mathbf{q}_0,1},n_{\mathbf{q}_0,2},\ldots,n_{\mathbf{q}_{N-1},1},n_{\mathbf{q}_{N-1},2}\rangle \equiv |\mathbf{k},dc,n\rangle \otimes |n_{\mathbf{q}_0,1},n_{\mathbf{q}_0,2},\ldots,n_{\mathbf{q}_{N-1},1},n_{\mathbf{q}_{N-1},2}\rangle, \tag{14}$$

where the wave function is expressed as the product of a vibron involving the high-energy mode and a vibrational wave function written in the phonon number basis set $n_{\mathbf{q}_{i,\alpha}}$, indicating the number of low energy phonons delocalized over molecules of type α with wave vector $\mathbf{q}_i$. When the high energy mode is neglected vibronic states are replaced by free exciton states $|\mathbf{k},dc\rangle$, labeled only by their wave vector and Davydov component, having an energy dispersion $E^{\mathrm{exc}}_{\mathrm{dc}}(\mathbf{k})$ given by the already mentioned purely excitonic bands. This can be formally obtained from Hamiltonians (3) or (11) by setting $\lambda_1=0$.

Hamiltonian (3) and, of course, Hamiltonian (11) are invariant under translations by a lattice vector and under screw symmetry, so that the total wave vector $\mathbf{K}$ of the dressed exciton plus the low energy phonons are conserved, as well as the parity under a twofold rotation around the b axis. Since we are interested in normal incidence absorption spectra, in the following we will only consider crystal states with $\mathbf{K}=0$. Such a subspace can be further decomposed into two decoupled subspaces with A and B symmetries, which are responsible for b-polarized and a-polarized absorptions, respectively. Crystal states with A and B symmetries can be built from any given state ψ as

$$\psi^{(b)} = \frac{1}{\sqrt{2}}(\psi + \hat{O}\psi), \quad \psi^{(a)} = \frac{1}{\sqrt{2}}(\psi - \hat{O}\psi), \tag{15}$$

respectively, where $\hat{O}$ denotes the screw symmetry operator. The effect of $\hat{O}$ on a state $\psi=|\mathbf{k},dc,n\rangle \otimes |n_{\mathbf{q}_0,1},n_{\mathbf{q}_0,2},\ldots,n_{\mathbf{q}_{N-1},1},n_{\mathbf{q}_{N-1},2}\rangle$ is to change it into $\hat{O}\psi = (\hat{O}|\mathbf{k},dc,n\rangle) \otimes |n_{\hat{O}\mathbf{q}_0,2},n_{\hat{O}\mathbf{q}_0,1},\ldots,n_{\hat{O}\mathbf{q}_{N-1},2},n_{\hat{O}\mathbf{q}_{N-1},1}\rangle$, where $\hat{O}|\mathbf{k},dc,n\rangle = |\hat{O}\mathbf{k},dc,n\rangle$ if $\hat{O}\mathbf{k}\neq\mathbf{k}$ and $\hat{O}|\mathbf{k},dc,n\rangle = \pm|\mathbf{k},dc,n\rangle$ if $\hat{O}\mathbf{k}=\mathbf{k}$, the sign depending on the parity of the Davydov component dc. In our numerical calculations we always used symmetry adapted basis sets so that we could diagonalize the Hamiltonian for each subspace separately obtaining the crystal eigenstates $\psi^{(j)}_n$ and their energies $E^{(j)}_n$ for both polarizations, $j=\{a,b\}$. The corresponding complex refractive indices $n_j(\omega)=\sqrt{\epsilon_j(\omega)}$ and absorption coefficients $\alpha_j(\omega)=2\Im[n_j(\omega)]\omega/c$ have finally been computed from the 2D dielectric constant $\epsilon_j(\omega)$. The latter, due to crystal symmetry, is diagonal in the ab frame of reference and it is explicitly given by

$$\epsilon_j(\omega) = \epsilon_\infty + \frac{2}{\epsilon_0 \upsilon}\sum_n \frac{E^{(j)}_n|\mathbf{d}^{(j)}_n|^2}{(E^{(j)}_n)^2 - (\hbar\omega)^2 - i\gamma\hbar\omega}, \tag{16}$$

where υ is the unit cell volume, ϵ_∞ is the high frequency dielectric constant, γ is a damping factor which determines the width of the absorption line shape, and $\mathbf{d}^{(j)}_n = \langle\psi^{(j)}_n|\hat{\mathbf{d}}_j|0\rangle$,

$$\hat{\mathbf{d}}_j \equiv \sum_{\mathbf{n},\alpha,\tilde{\mu}} |\mathbf{n},\alpha,\tilde{\mu}\rangle\langle 0|S_{\tilde{\mu}0}\mathbf{d}_{\alpha,j} + \mathrm{H.c.} \tag{17}$$

being the projection along j of the dipole moment operator $\hat{\mathbf{d}}$, and $\mathbf{d}_{\alpha,j}$ the j component of molecule α dipole moment. In order to obtain a satisfactory agreement with the low-temperature (7 K) experimental results in the low energy region of the absorption spectrum, the damping factor γ, which in Eq. (16) has the units of energy, has been set to $\gamma = 0.003$ eV (about 24 cm^{-1}) for the b-polarized 0-0 origin and to 0.01 eV(80 cm^{-1}) for all the other states. The choice of an energy independent damping constant is justified by the limited spectral range we investigate, but it is worth mentioning that the above γ values are not correct in the high energy portion of the absorption spectrum. Moreover in all the calculations we used $\epsilon_\infty=2.1$ as in Ref. 18. We finally point out that the unit cell volume υ to be used in Eq. (16) is half the actual volume because our 2D unit cell contains two molecules instead of four.

B. Molecular interactions and excitonic bands

Molecular interactions inside the crystal are often approximated to be interactions between point dipoles located at the center of mass of each molecule. Such an approximation fails for molecules which are close to each other compared to their dimensions. In order to improve our estimate of such interactions, we replaced the delocalized molecular dipole with a distribution of point charges located at atomic positions as follows. First we used the GAUSSIAN 03 software[31] to perform a time dependent density functional calculation of the first molecular singlet transition. We

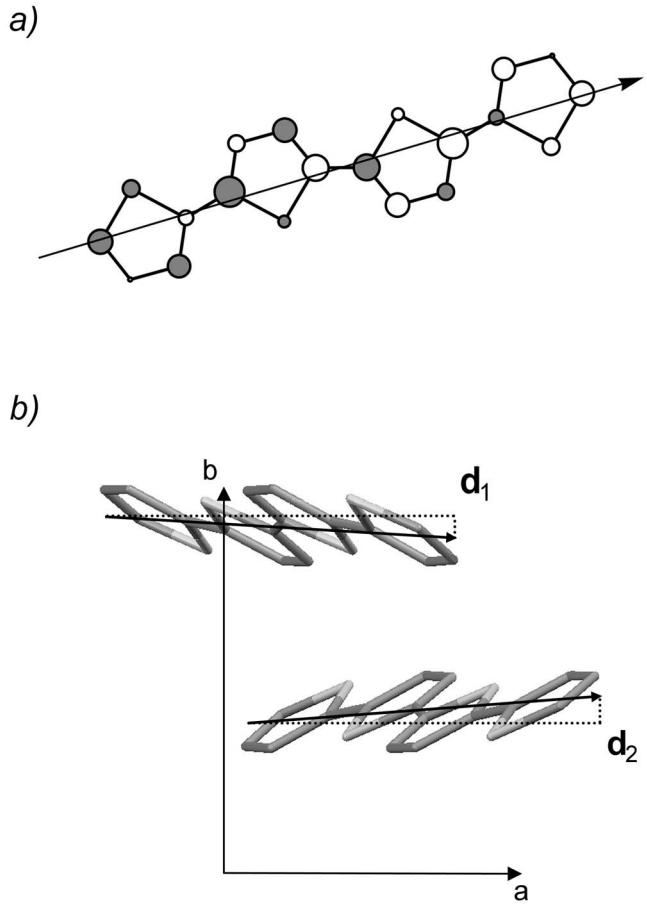

FIG. 1. (a) Distribution of the transition charge density for the first allowed molecular transition of 4T. Circle area is proportional to the atomic transition charge; color indicates a positive (white) or negative (gray) charge. The arrow indicates the direction of the total dipole moment, which is tilted by 3° with respect to the long molecular axis. (b) View of the 2D crystal unit cell along the c^* axis showing the herringbone arrangement of the molecular dipoles in the *ab* plane.

started from an optimized ground state geometry for the 4T molecule and employed a hybrid functional BLYP and 6-31G(D,P) basis set, finding that the first molecular electronic transition has a dipole moment of 10.6 D and that the highest occupied molecular orbital-lowest unoccupied molecular orbital (HOMO-LUMO) transition accounts for 73% of its oscillator strength. Then, we expressed the HOMO and LUMO wave functions as a sum of localized atomic orbitals and wrote the HOMO-LUMO transition dipole moment as the total dipole moment of a distribution of point charges localized on atomic sites.[32,33] In order to account for contributions from other orbitals, we finally normalized the dipole moment of the so obtained transition charge distribution to the computed transition dipole moment. The total dipole moments we obtained for the two inequivalent molecules are then $\mathbf{d}_1=4.37\hat{\mathbf{a}}-0.10\hat{\mathbf{b}}+9.62\hat{\mathbf{c}}^*$ D and $\mathbf{d}_2=4.37\hat{\mathbf{a}}+0.10\hat{\mathbf{b}}+9.62\hat{\mathbf{c}}^*$ D, respectively; the corresponding molecular transition charge distribution is reported in Fig. 1.

We also included isotropic screening so that the interaction between two molecules inside the crystal is finally given by

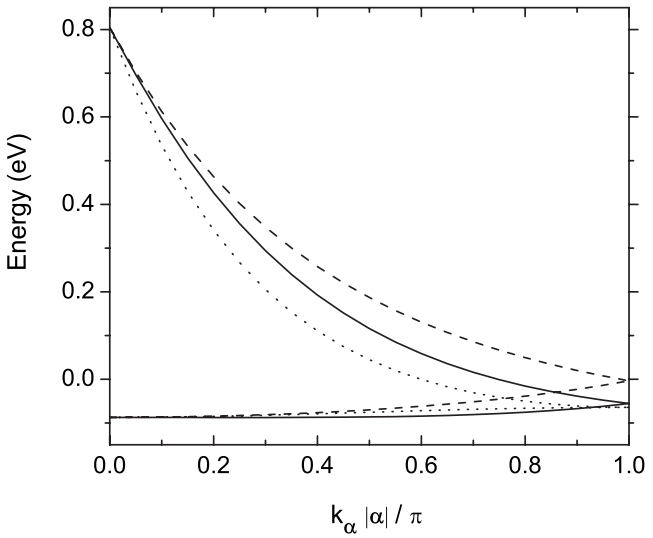

FIG. 2. Free exciton bands $E^{\mathrm{exc}}(\mathbf{k})$ in the first Brillouin zone computed for a 2D 4T crystal along $\mathbf{k}_\alpha \| \boldsymbol{\alpha}$ with $\boldsymbol{\alpha}=\mathbf{a}$ (solid line), **b** (dashed line), and **a** +**b** (dotted line).

$$J_{\alpha\beta}(\mathbf{n}-\mathbf{m})=\frac{1}{4\pi\epsilon_0\epsilon_s}\sum_{ij}\frac{q_{i\alpha}q_{j\beta}}{\delta r_{\mathbf{n}i\alpha,\mathbf{m}j\beta}}, \tag{18}$$

where ϵ_s is the static dielectric constant, chosen to be isotropic, $q_{i\alpha}$ is the transition charge located on the ith atom of the αth molecule, and $\delta r_{\mathbf{n}i\alpha,\mathbf{m}j\beta}$ is the distance between the ith atom of the αth molecule in cell **n** and the jth atom of the βth molecule in cell **m**. The calculation of $\tilde{J}_{\alpha\beta}(\mathbf{k})$ is straightforward, since in a 2D crystal the infinite summation can be estimated to the desired accuracy with a finite number of cells. In our calculations we used $\epsilon_s=2.76$, which is the value we extrapolated from UV-visible reflectivity measurements at near normal incidence with *b*-polarized light. Indeed, in this configuration, reflectivity R only depends on the b component ϵ_s of the diagonal dielectric tensor as $R=|(\sqrt{\epsilon_s}-1)/(\sqrt{\epsilon_s}+1)|^2$. The reflectivity in the transparency region below 2 eV was found to be 0.062 from which ϵ_s was deduced. These new reflectivity measurements have been performed using a substrate with an appropriate refractive index in order to reduce the contribution of multiple reflections from the back face of the sample, which, on the contrary, affects reflectance data reported in the literature[20] in the low energy region (below 3.5 eV). The computed free exciton bands, which are the eigenvalues of the $\tilde{J}_{\alpha\beta}(\mathbf{k})$ 2×2 matrix as a function of **k**, are reported in Fig. 2. The purely excitonic DS is found to be 0.89 eV, in good agreement with previous experimental and theoretical works,[14,19,17] while the lower band has a maximum width of 0.084 eV or 677 cm^{-1} along k_b, which is compatible with the lower bound of 100 cm^{-1} estimated by Gebauer *et al.*[13]

A more accurate approximation would require taking into account an anisotropic static dielectric tensor with one principal axis along b and the other two in the *ac* plane. In particular we expect the static dielectric constant corresponding to the principal axis closer to c to be larger than the value of 2.76 measured along b. Nevertheless, we will show in Sec. III that our numerical calculations reproduce the correct

experimental splitting between the *b*-polarized absorption origin at 2.6 eV and the most intense absorption peak at 3.7 eV as measured at normal incidence. From the above discussion we deduce that introducing an anisotropic screening would lower interactions with respect to our calculations; on the other hand a more accurate description of screening, which is not effective between nearest neighbors, would enhance molecular interactions and the two corrections will largely cancel each other at $\mathbf{k}=0$ in order to give again the correct experimental DS. We have done some numerical simulations using anisotropic screening and we indeed found that the band structure is barely affected by the above refinements.

In order to check the 2D approximation, we have also computed the full 3D bands for an infinite crystal by using the transition charge formalism in combination with the Ewald method. First, we mention that we obtained very flat bands along the c^* direction, the full width being less than 0.006 eV for all the four bands. Focusing now on the *ab* plane dispersion and having in mind the 2D bands, we found that interplane interactions produce a splitting of each allowed band into an allowed and a dark band. In particular, at $\mathbf{k}^{3D}\approx 0$, with $\mathbf{k}^{3D}$ along c^*, we computed a splitting of about 0.01 eV for the lower band and a total increase in the DS by less than 1%. However, the line shapes and splittings of the *ac*- and *b*-polarized components of the 0-1 replicas depend primarily on the relative values of $\lambda_0^2\hbar\omega_0$ and the lower bandwidth. Since the change induced to the latter is small, particularly when the high energy mode is included, the splitting of the *ac*- and *b*-polarized components of the 0-1 replicas is dominated by 2D interactions and only slightly reduced by interplane interactions.

III. NUMERICAL RESULTS FOR THE LOW ENERGY ABSORPTION SPECTRUM OF 4T

We computed the normal incidence absorption spectra in the low energy region for crystals of different sizes $N=N_a\times N_b$ and found that by increasing N we could achieve a fairly good convergence to a limit which can be considered as the infinite crystal absorption spectrum. In order to work with a finite basis set we had to set a maximum number of allowed vibrational quanta for each basis state, denoted as M_0 and M_1 for the low and the high energy vibrational modes, respectively. We mention that for a crystal composed of N cells the number of basis states with a given total wave vector $\mathbf{K}$ scales, for large N, as $(M_1+1)N^{M_0}$. In our calculations we always used $M_0=3$ and $M_1=4$ which were large enough to ensure convergence at all crystal sizes. As already discussed, by using symmetry adapted crystal states the BO basis could be split into two uncoupled sets, producing the *b*-polarized and *a*-polarized parts of the normal incidence absorption spectrum, respectively. The maximum number of basis states we could handle was about 220 000 for each polarization. The corresponding Hamiltonian has been diagonalized by means of the Arnoldi/Lanczos algorithm, which, for the largest basis sets, allowed us to compute the first 500 eigenvalues and eigenvectors.

In all our numerical calculations we used the following parameters: $\hbar\omega_{0-0}+D=2.64$ eV, $\hbar\omega_0=161\ \mathrm{cm}^{-1}=0.02$ eV,[16] $\hbar\omega_1=1470\ \mathrm{cm}^{-1}=0.18$ eV,[14,18] and, unless explicitly stated, HR factors have been both set to unity, i.e., $\lambda_0=1$ and $\lambda_1=1$, as done in previous works.[9,14,29]

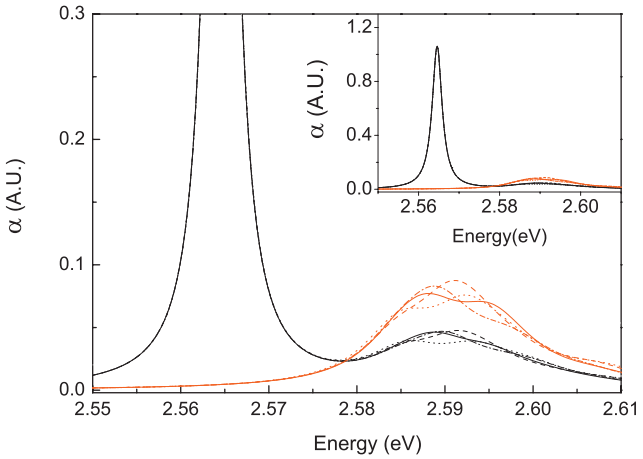

FIG. 3. (Color) Absorption spectrum of a 4T crystal computed including a single low energy mode for different crystal sizes ($N_a\times N_b$): 4×4 (dotted line), 5×5 (dashed line), 6×6 (dashed-dotted line), and 7×7 (solid line). Black (red) lines indicate the *b*-polarized (*a*-polarized) component of the spectrum. Inset: The same spectra in a different scale.

A. Single low energy intramolecular mode

We will first discuss the crystal absorption when only the low energy intramolecular mode is present. As already shown, the computed free exciton DS is $W=0.89$ eV, which compares well with previous works.[14] The lower exciton bandwidth is $\Delta=0.084$ eV, leading to the inequality $W\gg\frac{4}{\pi}\Delta>\lambda_0^2\hbar\omega_0$, which describes a weak or, at most, intermediate-I EP coupling regime. The low energy portion of the absorption spectra computed for crystals of increasing sizes is reported in Fig. 3. We found a size independent *b*-polarized (0-0) origin at 2.565 eV followed by two (0-1) replicas with different polarizations. The two replicas change their shape as the crystal size is increased, but their center of gravity does not move and, in addition, the shape is clearly the same for both polarizations with a splitting always less than 1 meV or 8 cm^{-1}, as expected for a crystal obeying a weak EP coupling regime. Nevertheless, for the largest investigated crystal, replica maxima are located at 190 and 195 cm^{-1}, respectively, above the absorption origin, i.e., significantly higher in energy with respect to the one vibrational quantum shift (161 cm^{-1}) one would expect in the weak EP regime. Another interesting feature of the predicted spectrum is that the replicas consist of two well defined peaks instead of wide absorption bands. Both these features are typical of the intermediate-I regime, as we will discuss below. Further increasing the size of the crystal beyond 49 cells was not possible on our workstation, but we do not expect any significant change in the general features of the spectra with respect to the ones shown in the figure.

We can explore other coupling regimes by changing the HR factor λ_0^2 and measuring the relative positions of the first three absorption peaks. In the following we will denote $\delta(\beta)$

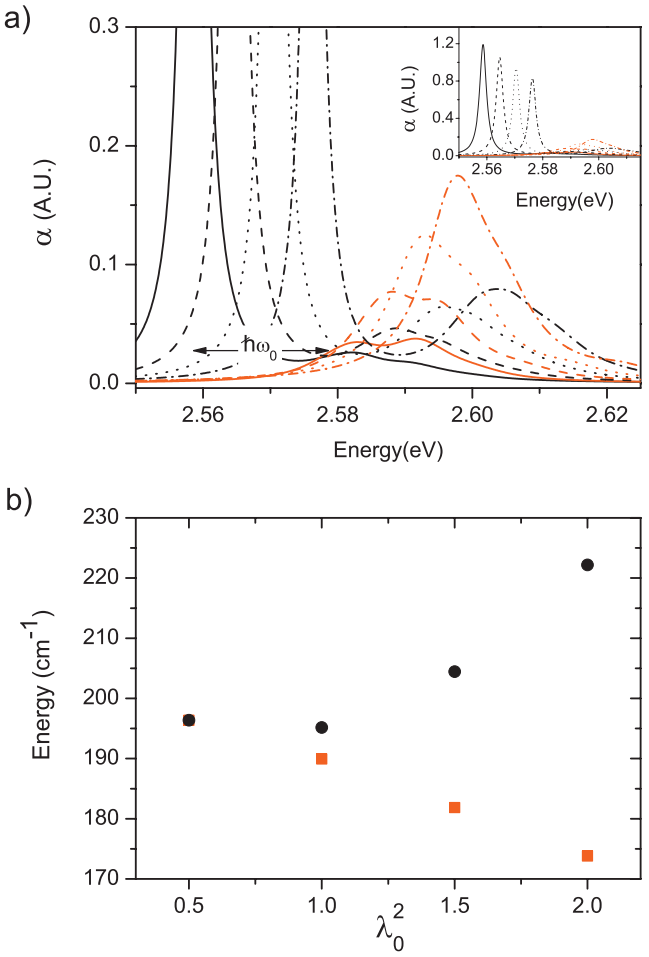

FIG. 4. (Color) (a) Absorption spectra for a 7×7 cell 4T crystal computed including a single low energy mode with $\lambda_0^2=0.5$ (solid line), 1 (dashed line), 1.5 (dotted line), and 2 (dashed-dotted line). Black (red) lines indicate the *b*-polarized (*a*-polarized) component of the spectrum. Inset: The same spectra in a different scale. (b) Spectral shifts δ (black circles) and β (red squares) as a function of λ_0^2. The value of β at $\lambda_0^2=0.5$ refers to the position of the lowest energy peak.

as the spectral difference between the maximum of the first *b*-polarized (*a*-polarized) replica and the *b*-polarized origin. Figure 4 shows the results for a 7×7 crystal with λ_0^2 ranging from 0.5 to 2. We clearly see that by increasing λ_0 we move toward the intermediate-I regime, where the two replicas split. Moreover, when $\lambda_0^2\geq1$, both δ and β have a nearly linear dependence on λ_0^2 and they split almost symmetrically with respect to the value $\delta=\beta=193$ cm^{-1}.[9] As λ_0 increases we also find that oscillator strength is transferred from the (0-0) origin to the (0-1) replicas. By decreasing λ_0^2, on the contrary, we go further into the weak coupling regime: At $\lambda_0^2=0.5$, for instance, the splitting vanishes and each replica has a small peak intensity and a low energy edge lying exactly one vibrational quantum above the origin, as explicitly shown in Fig. 4(a).

All of the above behaviors are in good agreement with the predictions of the aggregate model[9] and can be explained by explicitly writing down the states involved in the absorption process. In the weak coupling regime the (0-0) origin is mainly due to the state $\psi_{0\text{ph}}^{(b)}=|\mathbf{k}=0,\ dc=L\rangle\otimes|0,\ldots,0\rangle$, while the other dipole-allowed 0 phonon state $\psi_{0\text{ph}}^{(a)}=|\mathbf{k}=0,\ dc=U\rangle\otimes|0,\ldots,0\rangle$ is 0.89 eV higher in energy (L and U denote lower and upper Davydov bands, respectively). Replicas are built from symmetry adapted combinations of BO states

$$\psi_{1\text{ph},\mathbf{k}}^{(b)}=\frac{1}{\sqrt{2}}[|\mathbf{k},L\rangle\otimes b_{-\mathbf{k},1}^{\dagger}|0,\ldots,0\rangle+(\hat{O}|\mathbf{k},L\rangle)\otimes b_{-\hat{O}\mathbf{k},2}^{\dagger}|0,\ldots,0\rangle], \tag{19}$$

$$\psi_{1\text{ph},\mathbf{k}}^{(a)}=\frac{1}{\sqrt{2}}[|\mathbf{k},L\rangle\otimes b_{-\mathbf{k},1}^{\dagger}|0,\ldots,0\rangle-(\hat{O}|\mathbf{k},L\rangle)\otimes b_{-\hat{O}\mathbf{k},2}^{\dagger}|0,\ldots,0\rangle], \tag{20}$$

where $\mathbf{k}$ denotes the excitonic wave vector and we stress that the total wave vector of all the states involved in the absorption process is $\mathbf{K}=0$. States $\psi_{1\text{ph},\mathbf{k}}^{(b)}$ and $\psi_{1\text{ph},\mathbf{k}}^{(a)}$ are optically allowed through a weak HT coupling to the allowed states $\psi_{0\text{ph}}^{(b)}$ and $\psi_{0\text{ph}}^{(a)}$, respectively, but the coupling is so weak that the energy can be assumed to be $E_L^{\text{exc}}(\mathbf{k})+\hbar\omega_0$ for both states. As a consequence, the two replicas are nearly degenerate and the absorption line shapes are determined by two factors: The oscillator strength of states (19) and (20) and the excitonic density of states. Applying first order perturbation theory we find that the oscillator strength scales as $(\hbar\omega_0)^2/(E_L^{\text{exc}}(\mathbf{k})+\hbar\omega_0)^2$ and as $(\hbar\omega_0)^2/(W-E_L^{\text{exc}}(\mathbf{k})-\hbar\omega_0)^2$ for states $\psi_{1\text{ph},\mathbf{k}}^{(b)}$ and $\psi_{1\text{ph},\mathbf{k}}^{(a)}$, respectively. From the above expressions we see that among *b*-polarized states (19), oscillator strength is predicted to be larger for low energy states; an opposite behavior is instead predicted for *a*-polarized states (20). This explains why for $\lambda_0^2=0.5$ in the *b*- and *a*-polarized replicas the most intense peak is found to be the low (high) energy one, as in Fig. 4(a). As for the free exciton density of states, we find that it is nearly constant starting from the band bottom energy up to a point 0.02 eV above it, where it has a small peak and then it drops at higher energies. From the above results we expect that in the weak coupling regime, replicas consist of weak, degenerate absorption bands with a width of the order of 0.02 eV and a lower edge lying 161 cm^{-1} above the 0-0 origin. When the EP coupling increases, interaction between states $\psi_{1\text{ph},\mathbf{k}}^{(b)}$ or $\psi_{1\text{ph},\mathbf{k}}^{(a)}$ cannot be treated as a weak perturbation and it gives rise to a single dominant peak for each replica. This peak draws most of the oscillator strength, producing a narrowing of the linewidths and, eventually, the splitting between replicas. We can now explain why, even when $\lambda_0^2=0.5$ and there is no splitting, δ differs from 161 cm^{-1}. States $\psi_{1\text{ph},\mathbf{k}}^{(b)}$ with large wave vectors $\mathbf{k}$ are responsible for this behavior since due to the small excitonic band curvature, EP coupling is still strong enough to provide them with a non-negligible oscillator strength. A similar reasoning applies to *a*-polarized states, explaining the enhanced value of β.

B. Two intramolecular modes

We now add a high energy vibrational mode with $\hbar\omega_1=1470$ cm^{-1} and $\lambda_1^2=1$. The energy of the mode has been chosen, as in previous works,[14,18] to represent an effective mode describing the room temperature spectrum of 4T crys-

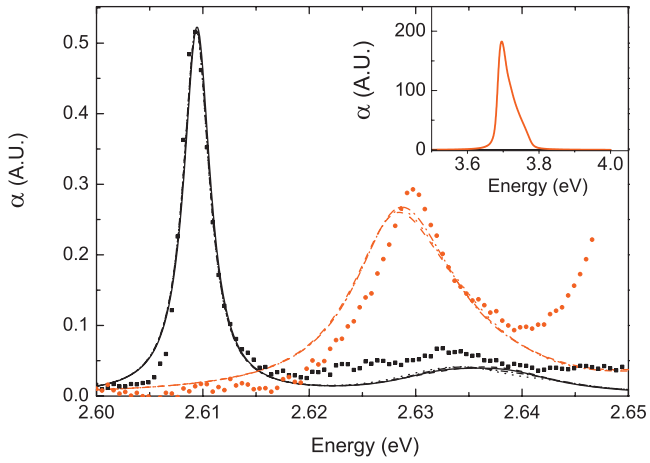

FIG. 5. (Color) Absorption spectrum of a 4T crystal computed including two modes for different crystal sizes ($N_a \times N_b$): 3×3 (dotted line), 4×4 (dashed line), 5×5 (dashed-dotted line), and 6×6 (solid line). The experimental spectrum of sample B from Ref. 11 is also shown for comparison with full symbols. Black (red) lines and symbols indicate the *b*-polarized (*a*-polarized) component of the spectrum. In the inset we report the high energy part of the spectrum computed for a 3×3 crystal, showing a very intense *a*-polarized absorption peak at 3.7 eV.

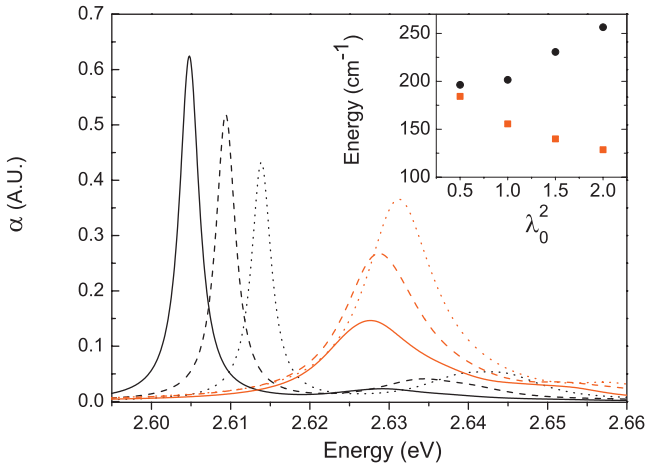

FIG. 6. (Color) Absorption spectra for a 5×5 4T crystal computed including two vibrational modes with $\lambda_1^2=1$ and $\lambda_0^2=0.5$ (solid line), 1 (dashed line), and 1.5 (dotted line). Black (red) lines indicate the *b*-polarized (*a*-polarized) component of the spectrum. Inset: Spectral shifts δ (black circles) and β (red squares) as a function of λ_0^2.

tals. The impact of changing the HR factor, on the contrary, will be discussed in the following. The most important effect of adding the high energy mode is to drive the crystal toward the intermediate-I or even the strong-I regime, as it can be seen at first glance by comparing the total molecular relaxation energy $\lambda_0^2\hbar\omega_0+\lambda_1^2\hbar\omega_1 \approx 1630$ cm^{-1} with $\frac{4}{\pi}\Delta \approx 860$ cm^{-1}. The low energy absorption spectra for crystals with sizes up to 5×5 cells are shown in Fig. 5. In the same figure we also added the *b*-polarized absorption spectrum of a 6×6 cell crystal (black solid line) obtained by means of a very good approximation which includes only the lowest energy vibronic states in both polarizations, as described in detail in Sec. IV.

It is evident from the figure that the predicted splitting between replicas is now very large. Moreover, the convergence with size is improved with respect to the single mode calculations, as it can be seen by comparing Figs. 3 and 5. Our numerical results are compared in Fig. 5 with the low-temperature (7 K) experimental absorption spectra of sample B from Ref. 11, assuming a sample thickness of 800 nm, in agreement with an experimental value of the order of several hundred nanometers. The theoretical splitting between maxima is 46 cm^{-1} for the 5×5 crystal, larger than the experimental value of about 23 cm^{-1}, but the main features of the spectrum are clearly reproduced. In the inset we report the high energy absorption of the 3×3 crystal, only to show that the position of the most intense absorption peak is correctly predicted at 3.7 eV. This observation, together with the *b*-polarized origin at 2.61 eV, confirms that the choice of an isotropic static dielectric constant, combined with our calculation of the screened molecular interactions, gives meaningful results. We clarify that the reason why the absorption coefficient reported in the high energy region is unrealistically large is our choice of the damping factor $\gamma=0.01$ eV, which is too small to account for the many phonon modes that come into play at high energies. Failure to reproduce the high energy tails of the replicas is instead a consequence of the limited number of states we could include in our calculations.

In summary we can say that the calculated low energy absorption compares well with the experimental spectrum. The predicted splitting between (0-1) replicas is actually larger than the measured one, ranging between 18 and 23 cm^{-1} for different samples when considering the position of the maxima,[11] but we stress that we did not take into account the disorder. In addition, the actual HR factors could be different from the one we used in Fig. 5. In particular, very recent experimental and theoretical results[34] indicate that λ_0^2 could be 0.5 or even smaller. In the former case, for instance, the computed absorption spectra can be seen in Fig. 6 and the corresponding splitting is found to be about 12 cm^{-1}. From our results we can draw two important conclusions. First, the 4T crystal can be described by the intermediate-I regime, which unambiguously predicts peaked split replicas. Second, we demonstrate that the high energy effective mode is crucial in driving the system into this EP coupling regime. A very simple way of describing the role of the high energy mode is by noting that it renormalizes the free exciton bands so that the low energy mode couples to vibrons which are much heavier than free excitons, the effective lower Davydov bandwidth becoming approximately $\Delta e^{-\lambda_1^2}$. This point will be discussed in more detail in Sec. IV.

We also investigated the effect of the two HR parameters on the relative positions of the low energy absorption peaks, as already done in Sec. III A. In Fig. 6 we report the absorption spectra of a 5×5 cell crystal, together with δ and β for different values of λ_0^2, while keeping $\lambda_1^2=1$ constant. We notice that the behavior is similar to the one observed in Sec. III A with the difference that we need smaller λ_0^2 values to reach the weak EP coupling limit.

In Fig. 7 we report instead the absorption spectra for a 5×5 cell crystal, together with δ and β for different values of λ_1^2, while keeping $\lambda_0^2=1$ constant. The single mode results (for a 5×5 cell crystal) are recovered at $\lambda_1=0$ and there is a

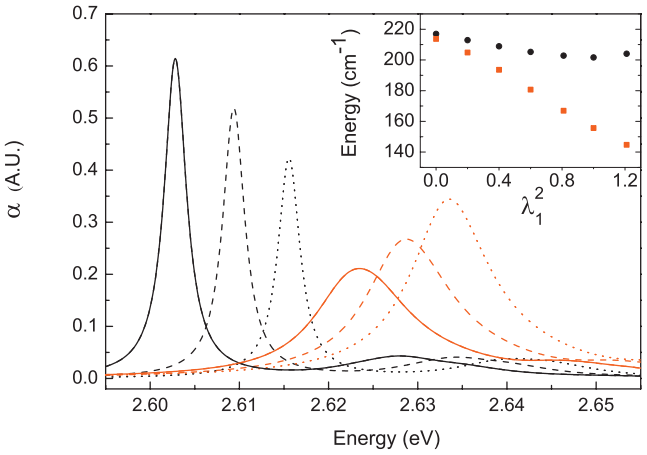

FIG. 7. (Color) Absorption spectra for a 5×5 4T crystal computed including two vibrational modes with $\lambda_0^2=1$ and $\lambda_1^2=0.8$ (solid line), 1.0 (dashed line), and 1.2 (dotted line). Black (red) lines indicate the *b*-polarized (*a*-polarized) component of the spectrum. Inset: δ (black circles) and β (red squares) as a function of λ_1^2.

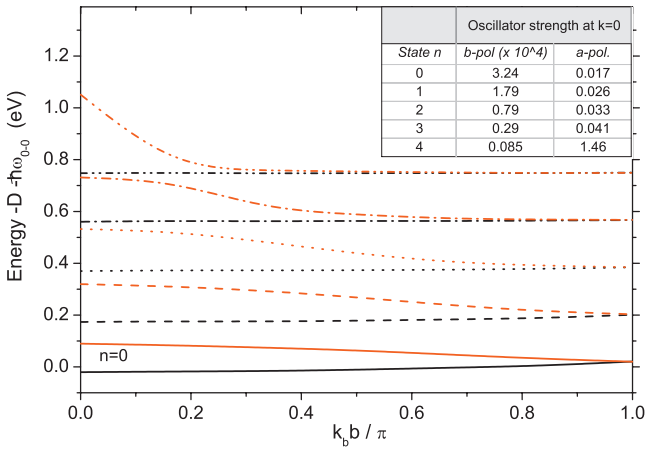

FIG. 8. (Color) Vibronic bands $E_{dc,n}^{\mathrm{vib}}(\mathbf{k})$ computed along k_b including up to four high energy vibrations. We report both lower *b*-polarized (black lines) and upper *a*-polarized (red lines) Davydov bands corresponding to $n=0,\ldots,4$ (solid lines) in order of increasing energy. In the table we report the oscillator strength of the dipole allowed vibronic states at $\mathbf{k}=0$.

large increase in the δ-β splitting as λ_1 gets larger, proving that coupling with the high energy mode is responsible for driving the system into the intermediate-I regime. It is also interesting that in this case, β decreases linearly with λ_1^2 while δ depends very weakly on it. At the same time, as λ_1 increases, oscillator strength is transferred from the origin to the *a*-polarized replica, while the *b*-polarized replica is not changing in intensity.

IV. ANALYSIS OF THE TWO-MODE NUMERICAL RESULTS

Numerical absorption spectra obtained by the two mode calculations can be explained by considering the two mode problem as a single mode problem in which free excitons are replaced by vibrons. By adopting this point of view we can exploit the results of the detailed analysis of the single mode aggregate model presented in our previous work.[9] As an aid to the following discussion, the vibronic band dispersion along k_b has been computed by diagonalizing the vibronic Hamiltonian H_{vib} of Eq. (4) and reported in Fig. 8 for $\lambda_1=1$. The main difference with the single mode case is that the oscillator strength is now distributed among many allowed purely vibronic states, namely, $\psi_{0\mathrm{ph},n}^{(b)}=|\mathbf{k}=0,\ dc=L,n\rangle\otimes|0,\ldots,0\rangle$ and $\psi_{0\mathrm{ph},n}^{(a)}=|\mathbf{k}=0,\ dc=U,n,\rangle\otimes|0,\ldots,0\rangle$, where *n* labels states in order of increasing energy. The *b*-polarized origin in this case is mainly due to the state $\psi_{0\mathrm{ph},n=0}^{(b)}$, while the *a*-polarized state carrying the most oscillator strength is, in our numerical calculations, $\psi_{0\mathrm{ph},n=4}^{(a)}$. The biggest contribution to the (0-1) replica absorption comes from states

$$\psi_{1\mathrm{ph},\mathbf{k}}^{(b)}=\frac{1}{\sqrt{2}}[|\mathbf{k},L,n=0\rangle\otimes b_{-\mathbf{k},1}^{\dagger}|0,\ldots,0\rangle + (\hat{O}|\mathbf{k},L,n=0\rangle)\otimes b_{-\hat{O}\mathbf{k},2}^{\dagger}|0,\ldots,0\rangle], \quad (21)$$

$$\psi_{1\mathrm{ph},\mathbf{k}}^{(a)}=\frac{1}{\sqrt{2}}[|\mathbf{k},L,n=0\rangle\otimes b_{-\mathbf{k},1}^{\dagger}|0,\ldots,0\rangle - (\hat{O}|\mathbf{k},L,n=0\rangle)\otimes b_{-\hat{O}\mathbf{k},2}^{\dagger}|0,\ldots,0\rangle], \quad (22)$$

which have total wave vector $\mathbf{K}=0$ and couple to the allowed purely vibronic states $\psi_{0\mathrm{ph},n}^{(b)}$ and $\psi_{0\mathrm{ph},n}^{(a)}$, respectively. Due to the reduced excitonic bandwidth ($\Delta^{\mathrm{vib}}=0.04$ eV) and to the increased relaxation energy, as compared to the single mode case, the coupling between $\psi_{1\mathrm{ph},\mathbf{k}}$ states and the purely vibronic states cannot be treated as a weak perturbation, not even for large wave vectors. In particular we find that states $\psi_{1\mathrm{ph},\mathbf{k}}^{(b)}$ and $\psi_{1\mathrm{ph},\mathbf{k}}^{(a)}$ are most strongly coupled to states $\psi_{0\mathrm{ph},n=0}^{(b)}$ and $\psi_{0\mathrm{ph},n=0}^{(a)}$, respectively. Due to the different energies of the vibronic states, such interactions produce a blueshift (redshift) of the *b*- (*a*)-polarized replica, thus giving rise to a noticeable splitting of the two absorption peaks. So far, we have not mentioned states with more than one low energy phonon, which, however, have been included in the calculations. Two phonon states, for instance, can be shown to push $\psi_{1\mathrm{ph},\mathbf{k}}$ states toward lower energies and their contribution cannot be neglected,[9] but their effect is nearly the same in both polarizations and that is why we preferred not to include them in the above discussion.

In order to check which vibronic states are responsible for the computed two mode absorption spectra, we plot in Fig. 9 (dotted line) the absorption spectrum of a 5×5 crystal computed by including, for each polarization, only the lowest energy vibronic band, i.e., neglecting all states with the vibronic quantum number $n>0$. This spectrum is compared to the spectrum obtained using the full basis (solid line) which includes all the vibronic bands. We find that the *b*-polarized spectrum is completely determined by the $n=0$ vibronic band, which is the one carrying nearly all the oscillator strength. On the other hand, the oscillator strength of the *a*-polarized replica is borrowed from all the allowed *a*-polarized vibronic states. This is clear from the dashed red line in Fig. 9, computed including both the lowest ($n=0$) and the highest ($n=4$) energy vibronic bands, which is still far

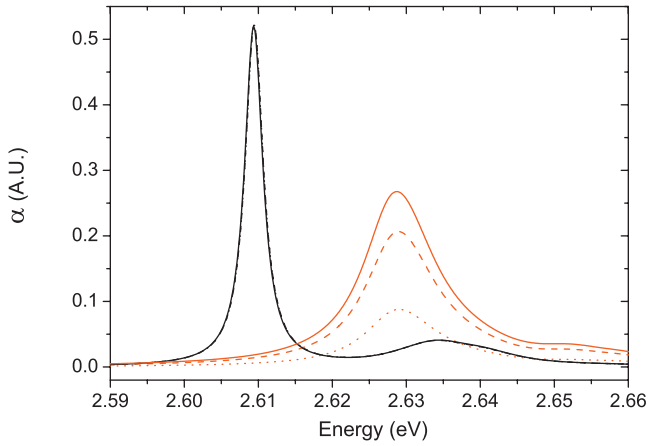

FIG. 9. (Color) Spectra calculated using a vibronic basis set and including only the lowest energy vibronic state ($n=0$) for each polarization (dotted line). We also show the results obtained by including both the lowest ($n=0$) and the highest ($n=4$) energy vibronic states for each polarization (dashed lines). The spectra calculated with the full basis ($n=0,\ldots,4$) are reported in solid line for comparison. Black (red) lines indicate the *b*-polarized (*a*-polarized) component of the spectrum.

from the exact spectrum (solid red line). It is very important to stress that on the contrary, the spectral position of the *a*-polarized replica is very well approximated by the single vibronic band approximation. This is because, as already mentioned, in the *a*-polarized subspace the (low-energy) one-phonon states are more strongly coupled to the nearby lowest energy vibron than to the other more intense vibronic states, much higher in energy. We can therefore conclude that the single vibronic band approximation is accurate enough to explain the spectral position of the low energy absorption peaks, even if it fails to describe the intensity of the *a*-polarized part of the spectrum.

The single vibronic band approximation can also explain the inset of Fig. 7. Plotting the vibronic energies at $\mathbf{k}=0$ as a function of λ_1^2 (Fig. 10), we see that the lowest energy *a*-polarized vibronic state moves very close to the *b*-polarized origin as λ_1^2 increases, while the spacing between *b*-polarized vibronic states remains nearly constant. This is why, correspondingly, δ stays nearly constant while β decreases significantly as λ_1^2 increases.

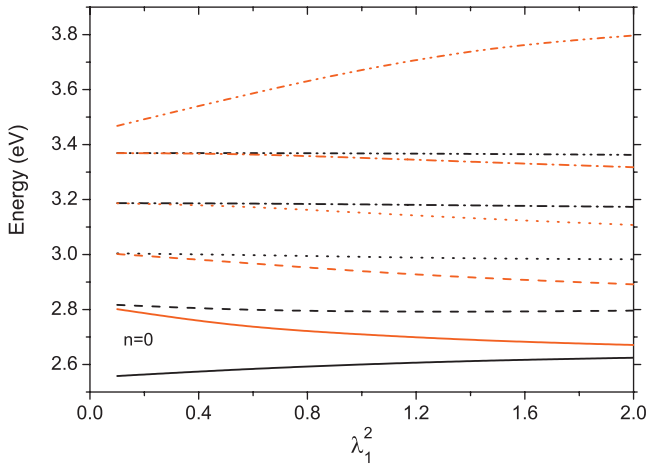

FIG. 10. (Color) Energy of the dipole allowed vibronic states $n=0,\ldots,4$ (solid lines) at $\mathbf{k}=0$ as a function of λ_1^2. Both *b*-polarized (black lines) and *a*-polarized (red lines) states are showed.

From our analysis we can conclude that adding the high energy mode has two combined effects: First, it reduces the lower band bandwidth by dressing the free exciton; second, it creates a new *a*-polarized dipole allowed vibronic state very close in energy to the *b*-polarized origin. The two effects produce a very large splitting between the first two replicas in the absorption spectrum.

We finally discuss the single particle approximation in treating the high energy mode. We believe that a single-particle approximation is enough to describe *b*-polarized dressed excitons, which are responsible for the renormalization of the lower Davydov excitonic band. On the other hand, we are aware that a single particle approximation is not accurate enough to describe *a*-polarized dressed excitons. In particular we expect that the use of a multiparticle approach would blueshift the lowest energy *a*-polarized dressed exciton state with respect to the vibronic approximation. This, in turn, would blueshift the spectral position of the *a*-polarized replica with respect to our calculations, bringing the spectra closer to the experimental results. Nevertheless, we feel that our approach is conceptually much simpler and numerically less intensive than a multiparticle treatment of the high energy mode.

V. CONCLUSIONS

In this work we have presented a theoretical model describing EP coupling in molecular crystals where two intramolecular vibrational modes are linearly coupled to crystal excitons. The model is quite general and it can be applied whenever one of the two modes is adequately described by a single particle approximation and the other is potentially in a weak to intermediate-I EP coupling regime. In fact, one of the modes is treated in the vibronic approximation while the other is described by a BO basis set. In the present paper, the model has been used to discuss the low energy portion of the absorption spectra of 4T crystals, as we found that it can be efficiently described by considering only two modes: A high energy effective mode at 1470 cm^{-1}, which represents the broad features of the whole absorption spectrum, and a low energy mode at 161 cm^{-1}, which is responsible for the fine details observable only at very low temperatures. The crystal has been considered as 2D mainly because of computational limitations with long-range molecular interactions modeled as Coulomb interactions between transition charge densities. The 2D approximation has been discussed in detail in Sec. II and we believe it captures the essential features of the problem for normal excitation to the *ab* plane[22] with a minor loss of accuracy, but it can be easily improved by implementing the numerical code on more powerful machines. Our numerical simulations, compared with experimental high resolution spectra, allowed us to draw some important conclusions. First, the two modes influence each other and it is not possible to treat each of them separately. Second, 4T crystals cannot be described by the conventional weak and strong EP coupling approximations, but they obey a new intermediate-I regime[9] which has a clear spectral signature. The synergy between the two modes has been demonstrated by showing the qualitative differences in the absorption spectra between

the two cases where a single low energy mode or both modes are considered. The effect of the high energy mode has been rationalized by describing the system in terms of a low energy mode coupled to high energy vibrons. This picture makes it easier to explain the main features of the absorption spectrum by simply considering a single mode problem where free excitonic bands are replaced by vibronic bands. In particular we found that the appearance of a new allowed *a*-polarized vibronic state at low energy, together with the overall rescaling of the bands, pushes the single low energy mode system out of the weak EP coupling regime into the intermediate-I regime. Foreseeable developments of this work will proceed in two main directions. The single-particle approximation for the high energy mode can be relieved by adding multiparticle states to the free exciton plus high-energy-phonon basis set. The model can be generalized to include more than two intramolecular vibrational modes.[35] Both these refinements will require a careful choice of the basis set and, probably, some clever approximation in order to keep the problem solvable with numerical methods.

ACKNOWLEDGMENTS

F.C.S. is supported by NSF, Grant DMR No. 0606028. L.S., S.T., P.S., and L.R. are supported by Fondazione Cariplo.

[1] G. Malliaras and R. H. Friend, Phys. Today **58**, 53 (2005).
[2] J. H. Burroughes, D. D. C. Bradley, A. R. Brown, R. N. Marks, K. Mackay, R. H. Friend, P. L. Burns, and A. B. Holmes, Nature (London) **347**, 539 (1990).
[3] S. R. Forrest, Nature (London) **428**, 911 (2004).
[4] H. Sirringhaus, N. Tessler, and R. H. R. H. Friend, Science **280**, 1741 (1998).
[5] C. J. Brabec, V. Dyakonov, J. Parisi, and N. S. Sariciftci, *Organic Photovoltaics: Concepts and Realization* (Springer, New York, 2003).
[6] W. T. Simpson and D. L. Peterson, J. Chem. Phys. **26**, 588 (1957).
[7] E. G. McRae, Aust. J. Chem. **14**, 329 (1961).
[8] E. G. McRae and W. Siebrand, J. Chem. Phys. **41**, 905 (1964).
[9] F. C. Spano, L. Silvestri, P. Spearman, L. Raimondo, and S. Tavazzi, J. Chem. Phys. **127**, 184703 (2007).
[10] The simplified model aggregate of Ref. 9 consists of a square lattice with lattice constant d and one molecule per cell. This is equivalent to a square lattice with two molecules per cell and lattice constant $a=d\sqrt{2}$, tilted by 45° with respect to the previous one. By unfolding the upper band in the second Brillouin zone, we can map the two band model into the single band model by simply rotating the wave vector space by 45°. Assuming isotropic parabolic bands $J_{\mathbf{k}}=J_c d^2k^2$ in the simplified model is therefore equivalent to having the dispersion $J_{\mathbf{k}}=(J_c/2)a^2k^2$ in the two band model, so that the maximum width of the lower band is $\Delta=J_c\pi^2$.
[11] L. Raimondo, M. Laicini, P. Spearman, S. Tavazzi, and A. Borghesi, J. Chem. Phys. **125**, 024702 (2006).
[12] T. Siegrist, C. Kloc, R. A. Laudise, H. E. Katz, and R. C. Haddon, Adv. Mater. **10**, 379 (1998).
[13] W. Gebauer, A. Langner, M. Schneider, M. Sokolowski, and E. Umbach, Phys. Rev. B **69**, 125420 (2004).
[14] X. H. Sun, Z. Zhao, F. C. Spano, D. Beljonne, J. Cornil, Z. Shuai, and J.-L. Bredas, Adv. Mater. **15**, 818 (2003).
[15] D. Fichou, G. Horowitz, V. Xu, and F. Garnier, Synth. Met. **48**, 167 (1992).
[16] D. Birnbaum, D. Fichou, and B. E. Kohler, J. Chem. Phys. **96**, 165 (1992).
[17] F. Kouki, P. Spearman, P. Valet, G. Horowitz, and F. Garnier, J. Chem. Phys. **113**, 385 (2000).
[18] M. Laicini, P. Spearman, S. Tavazzi, and A. Borghesi, Phys. Rev. B **71**, 045212 (2005).
[19] S. Tavazzi, M. Campione, M. Laicini, L. Raimondo, A. Borghesi, and P. Spearman, J. Chem. Phys. **124**, 194710 (2006).
[20] S. Tavazzi, A. Borghesi, M. Campione, M. Laicini, S. Trabattoni, and P. Spearman, J. Chem. Phys. **120**, 7136 (2004).
[21] F. Meinardi, M. Cerminara, A. Sassella, R. Bonifacio, and R. Tubino, Phys. Rev. Lett. **91**, 247401 (2003).
[22] F. C. Spano, Annu. Rev. Phys. Chem. **57**, 217 (2006).
[23] M. Muccini, M. Schneider, C. Taliani, M. Sokolowski, E. Umbach, D. Beljonne, J. Cornil, and J. L. Bredas, Phys. Rev. B **62**, 6296 (2000).
[24] P. F. van Hutten, J. Wildeman, A. Meetsma, and G. Hadziioannou, J. Am. Chem. Soc. **121**, 5910 (1999).
[25] C. C. Wu, M. C. Delong, Z. V. Vardeny, and J. P. Ferraris, Synth. Met. **137**, 939 (2003).
[26] A. S. Davydov, *Theory of Exciton* (Plenum, New York, 1971).
[27] P. Petelenz and M. Andrzejak, Chem. Phys. Lett. **343**, 139 (2001).
[28] P. Petelenz and M. Andrzejak, J. Chem. Phys. **113**, 11306 (2000).
[29] Z. Zhao and F. C. Spano, J. Phys. Chem. C **111**, 6113 (2007).
[30] T. Holstein, Ann. Phys. (San Diego) **8**, 325 (1959).
[31] M. J. Frisch, G. W. Trucks, H. B. Schlegel *et al.*, GAUSSIAN03, Revision C.01, Gaussian, Inc., Wallingford, CT, 2004.
[32] I. Vragovic and R. Scholz, Phys. Rev. B **68**, 155202 (2003).
[33] R. Scholz, A. Kobitski, T. Kampen, M. Schreiber, D. Zahn, G. Jungnickel, M. Elstner, M. Sternberg, and T. Frauenheim, Phys. Rev. B **61**, 13659 (2000).
[34] M. Andrzejak and M. T. Pawlikowski, J. Phys. Chem. A **112**, 13737 (2008).
[35] Z. Zhao and F. C. Spano, J. Chem. Phys. **122**, 114701 (2005).